JOURNAL OF SOLID STATE CHEMISTRY 110, 350–355 (1994)

The New Phosphates $Ln_{1/3}Zr_2(PO_4)_3$ (Ln = Rare Earth)

M. Alami Talbi and R. Brochu

Laboratoire de Chimie du Solide Appliquée, Faculté des Sciences, Avenue Ibn Batouta, Rabat, Morocco

and

C. Parent, L. Rabardel, and G. Le Flem

Laboratoire de Chimie du Solide du CNRS, Université Bordeaux I, 351 cours de la Libération, 33405 Talence Cedex, France

Received April 22, 1993; in revised form September 14, 1993; accepted September 17, 1993

The new phases $Ln_{1/3}Zr_2(PO_4)_3$ (Ln = Rare Earth) crystallize with the Nasicon-type structure. The rare earth is located in the usually labeled M_1 site with rather ionic Ln–O bonds. The ceramics resulting from the decomposition of these phosphates have been characterized in the case of lanthanum and europium. They exhibit a very low thermal expansion between room temperature and 1340°C. © 1994 Academic Press, Inc.

Since the pioneer work of Alamo *et al.* (1), Nasicon-type phosphates have been largely investigated as ultralow expansion ceramics.

The two prototype compositions are $NaZr_2(PO_4)_3$ [NZP] and $Ca_{0.5}Ti_2(PO_4)_3$ [CTP]. The crystal chemistry of this structure type allows an enormous range of cation substitution leading to a modulation of the thermal expansion coefficients along the **a** and **c** axes of the hexagonal cell. As the temperature increases, the correlated rotations of PO_4 tetrahedra and cation octahedra which constitute the framework are responsible for the opposed changes of parameters (2–6).

Actually, from a microscopic point of view, the main contribution to the thermal expansion of the skeletal framework of $M_xM_{1/2}(PO_4)_3$ phases involves the M–O bond (7). An empirical relation, given by Hazen *et al.*, allows calculation of its expansion coefficient: $\langle\alpha_{M-O}\rangle = 32.9(0.75 - Z/p) \times 10^{-6}\ °C^{-1}$ where Z and p are, respectively, the charge and the coordination number of the M atom.

For $x \leq 1$ the cations M^{n+} are assumed to be localized in the elongated distorted octahedron usually labeled M_1. In this context, low values of α_{M-O} can be expected if trivalent ions, e.g., rare earth, can be introduced in such sites.

With regard to these previous considerations, the present paper reports:

1. the preparation of the $Ln_{1/3}Zr_2(PO_4)_3$ phosphates through gel route, including a detailed study of the crystallization process;
2. the structural characterization of these new phases; and
3. the investigation of the thermal stability and the thermal expansion of $La_{1/3}Zr_2(PO_4)_3$ and $Eu_{1/3}Zr_2(PO_4)_3$ within a broad temperature range.

I. ELABORATION AND CRYSTALLIZATION OF GELS WITH $Ln_{1/3}Zr_2(PO_4)_3$ COMPOSITION

I.1. Gel Elaboration

The starting compounds Ln_2O_3 (Riedel de Haen) and $ZrOCl_2, 8H_2O$ (Riedel de Haen) were separately dissolved in 2 N HNO_3. The solutions were then mixed in stoichiometric proportions. The addition of a solution of $NH_4H_2PO_4$ under constant stirring produces a colorless gel except for neodymium and erbium, for which the gel colors are, respectively, violet and pink. The gel and supernatant solution mixture were maintained for 24 hr at 75°C and then progressively heated to 300°C. The thermal transformations of the obtained powders have been studied by DTA experiments and by using Eu^{3+} and Gd^{3+} as luminescent structural probes.

I.2. DTA Investigation

As an example, Fig. 1 presents the DTA of the sample with final composition $Eu_{1/3}Zr_2(PO_4)_3$ previously dried at 300°C. The first endothermic peak at 128°C is related to the evolving of both ammonia and nitrous vapors. This process is completely achieved at about 400°C. The crystallization starts at 800°C. XRD patterns with well-resolved lines can be recorded for samples annealed during a long time at this temperature (Fig. 2). The DTA peaks observed at high temperatures correspond to decomposition phenomena which begin at about 900°C. Ultimately

0022-4596/94 $6.00

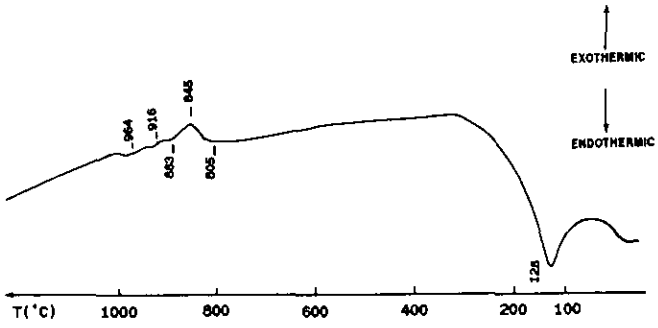

FIG. 1. Differential thermal analysis of a dried gel with $Eu_{1/3}Zr_2(PO_4)_3$ composition.

at 1300°C the phases β-$Zr_2P_2O_9$ and $LnPO_4$ appear and have been detected by XRD. The mechanism of this decomposition has been recently elucidated (14):

—below 1000°C the decomposition occurs without weight losses according to the reaction

$$Ln_{1/3}Zr_2(PO_4)_3 \rightarrow \tfrac{2}{3}ZrP_2O_7 + \tfrac{2}{3}Zr_2P_2O_9 + \tfrac{1}{3}LnPO_4;$$

—above 1000°C the zirconium diphosphate is then decomposed:

$$2ZrP_2O_7 \rightarrow Zr_2P_2O_9 + P_2O_5.$$

The overall process can be expressed by the equation

$$Ln_{1/3}Zr_2(PO_4)_3 \rightarrow Zr_2P_2O_9 + \tfrac{1}{3}LnPO_4 + \tfrac{1}{3}P_2O_5.$$

I.3. Crystallization Process Study Using Luminescent Probes

A parallel investigation of the crystallization process of $Eu_{1/3}Zr_2(PO_4)_3$ has been carried out by recording the $^5D_0 \rightarrow {}^7F_J$ (J = 0, 1, 2) emission of Eu^{3+} under a 360-nm excitation.

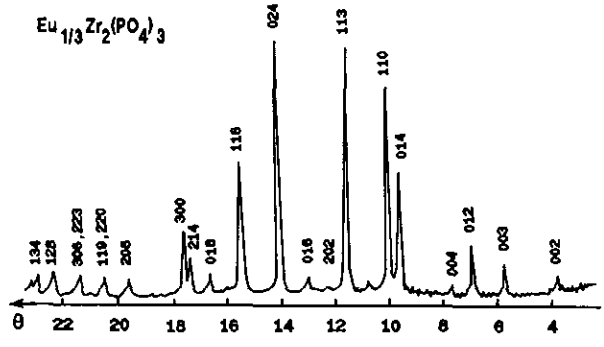

FIG. 2. X-ray diffraction spectrum of $Eu_{1/3}Zr_2(PO_4)_3$.

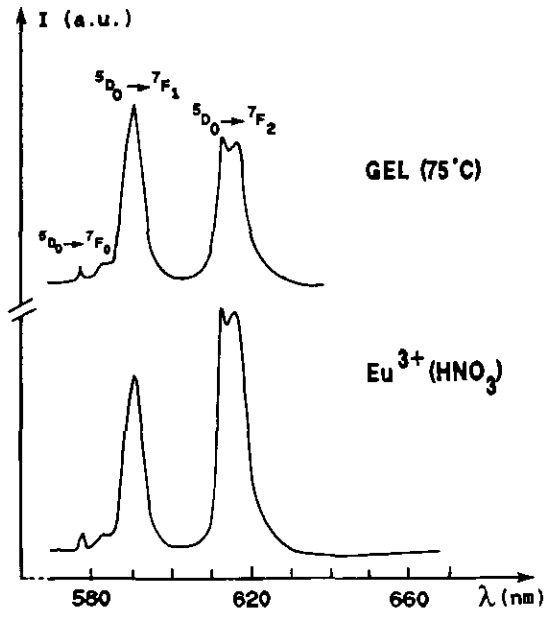

FIG. 3. Comparison of Eu^{3+} emission spectra for the $Eu_{1/3}Zr_2(PO_4)_3$ gel dried at 75°C and for the Eu^{3+} nitric solution (T = 300 K).

The emission spectrum of the gel dried at 75°C and more specifically the $^5D_0 \rightarrow {}^7F_0$ transition energy are identical to those of Eu^{3+} in the nitric solution, indicating a similar solvatation of this ion in both media (Fig. 3). After a treatment at higher temperatures, a broadening of all the emission bands is observed, as well as an increase of the intensity ratio

$$R = \frac{I^5D_0 \rightarrow {}^7F_2}{I^5D_0 \rightarrow {}^7F_1},$$

which increases from 2.6 to 4.2 between 200 and 600°C (Fig. 4). These results are consistent with the existence of a continuum of low symmetry sites for Eu^{3+} (19, 20).

The achievement of the crystallization at 800°C corresponds to a narrowing of all the $^5D_0 \rightarrow {}^7F_J$ lines. A unique $^5D_0 \rightarrow {}^7F_0$ line is observed at 17,355 cm^{-1} (Fig. 5).

The crystallization process of $Gd_{1/3}Zr_2(PO_4)_3$ can also be followed by recording the $^6P_{7/2} \rightarrow {}^8S_{7/2}$ emission of Gd^{3+} under a 274-nm excitation. Figure 6 exhibits the spectra of gels heated at increasing temperatures. Below 800°C a unique broad band is observed peaking at 312 nm. In contrast, the spectrum of the samples heated at 800°C contains three narrow lines peaking at 310.45, 311.45, and 312.90 nm (300 K) or 310.48, 311.45, and 312.86 nm (80 K) corresponding to the radiative deexcitation from the $^6P_{7/2}$ Stark components to the $^8S_{7/2}$ ground state (Fig. 7).

In conclusion, the crystallization of both phases with Eu and with Gd occurs at about 800°C.

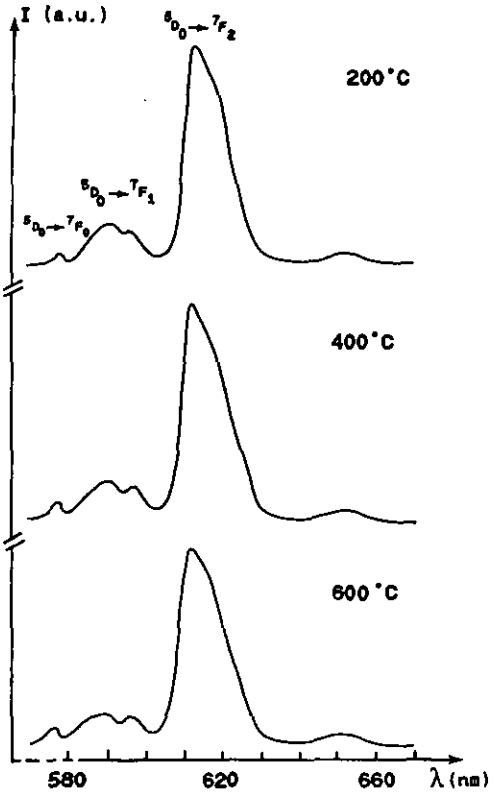

FIG. 4. $^5D_0 \rightarrow {}^7F_J$ Eu^{3+} emission for gels with $Eu_{1/3}Zr_2(PO_4)_3$ composition heated at 200, 400, and 600°C (λ_{exc} = 360 nm, T = 300 K).

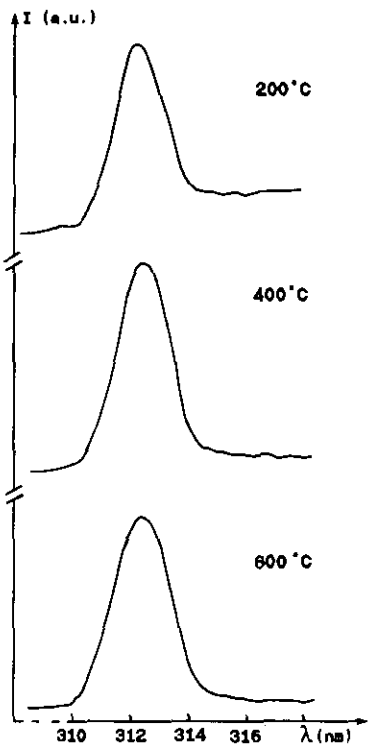

FIG. 6. $^6P_{7/2} \rightarrow {}^8S_{7/2}$ emission of Gd^{3+} for gels with $Gd_{1/3}Zr_2(PO_4)_3$ composition heated at 200, 400, and 600°C (λ_{exc} = 274 nm, T = 300 K).

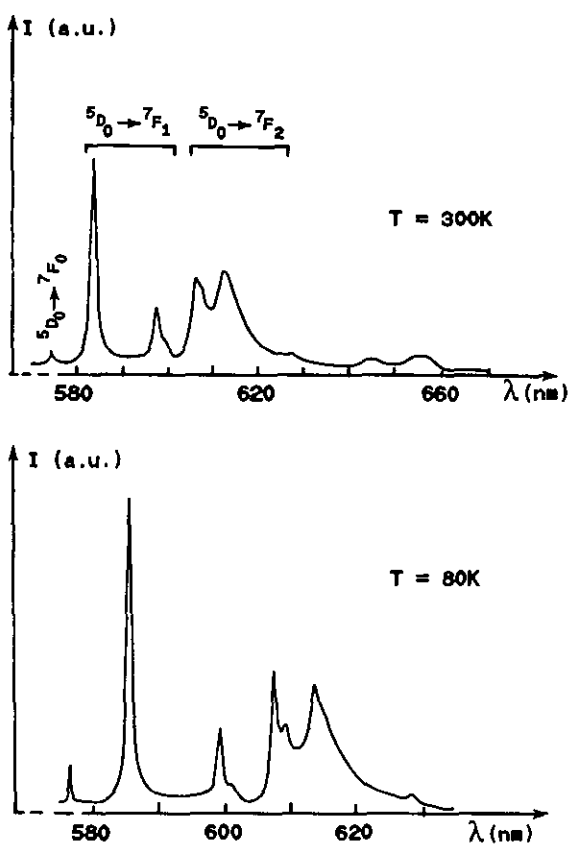

FIG. 5. $^5D_0 \rightarrow {}^7F_J$ emission of Eu^{3+} for the crystalline phase $Eu_{1/3}Zr_2(PO_4)_3$ (λ_{exc} = 360 nm, T = 80 and 300 K).

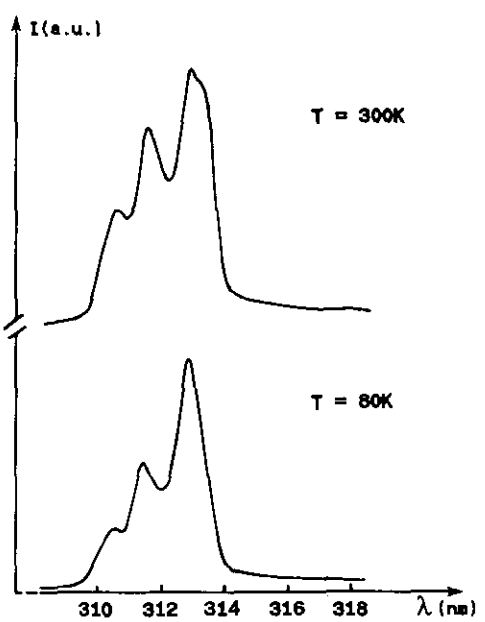

FIG. 7. $^6P_{7/2} \rightarrow {}^8S_{7/2}$ emission of Gd^{3+} for crystallized $Gd_{1/3}Zr_2(PO_4)_3$ recorded at 80 and 300 K (λ_{exc} = 274 nm).

TABLE 1
Cell Parameters of the $Ln_{1/3}Zr_2(PO_4)_3$ Phases (Ln = rare earth)

Ln^{3+}	r_i (Å)	(a_H ± 0.005) Å	(c_H ± 0.03) Å	(v_H ± 3) Å^3	c_H/a_H
La	1.06	8.741	23.21	1536	2.66
Pr	1.013	8.754	23.08	1532	2.64
Nd	0.995	8.762	23.04	1532	2.63
Sm	0.964	8.770	22.95	1529	2.62
Eu	0.95	8.767	22.91	1525	2.61
Gd	0.938	8.778	22.82	1523	2.60
Tb	0.923	8.780	22.82	1523	2.59
Er	0.881	8.796	22.64	1517	2.57
Tm	0.869	8.809	22.52	1513	2.56
Yb	0.858	8.808	22.48	1510	2.55

II. STRUCTURAL INVESTIGATION

The X-ray diffraction patterns can be indexed assuming a hexagonal cell (Table 1). The experimental densities measured for several samples imply six formula units in the unit cell (Table 2). The order of magnitude of these parameters is consistent with a Nasicon-type structure but the extinction rules exclude the $R\bar{3}c$ space group on account of the existence of the two lines corresponding to 7.56 and 5.70 Å. Similar lines previously observed in the case of $La_{0.33}Ti_2P_3O_{12}$ could be indexed by Senbhagaraman and Umarji by using the $R\bar{3}$ space group. This implies alternate vacancy and rare earth atom occupation along the hexagonal **c** axis (23).

The evolutions of the cell parameters as a function of the rare earth ionic radii are presented in Fig. 8. As the size of Ln^{3+} increases, a_H decreases whereas c_H increases. Similar behaviors have been observed for the families of the alkali or alkali-earth zirconium phosphates $AZr_2(PO_4)_3$ (A = Li, Na, K) (9–11) and $M'_{0.5}Zr_2(PO_4)_3$ (M' = Cd, Ca, Sr, Ba, Pb) (12–14).

The rare earth ions can be initially assumed to occupy the M_1 site of the $Ln_{1/3}Zr_2(PO_4)_3$ Nasicon structure. The lack of single crystals does not allow concluding to a random or ordered distribution.

According to Hagman *et al.* (10), the structural arrangement of $NaA_2(PO_4)_3$ consists of a three-dimensional framework formed by PO_4 tetrahedra sharing corners with AO_6 octahedra. The site occupied by the sodium atom, usually labeled M_1, is an elongated antiprism sharing triangular faces with the two neighboring AO_6 octahedra along the **c** axis of the hexagonal cell.

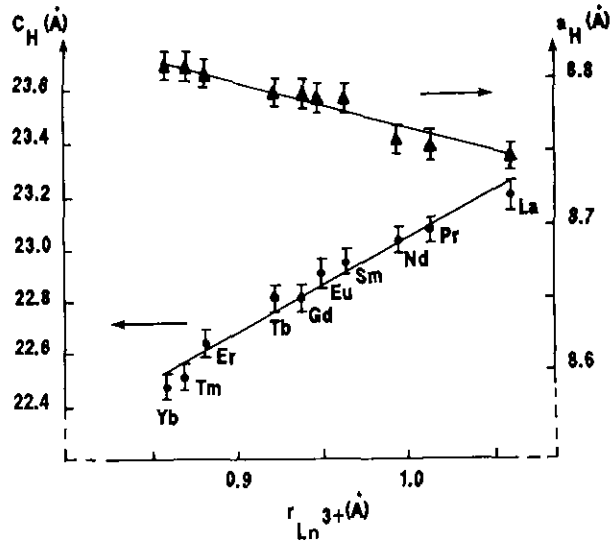

FIG. 8. Evolution of the cell parameters of the $Ln_{1/3}Zr_2(PO_4)_3$ phases vs Ln^{3+} ionic radii.

Table 3 compares the parameters of phosphates containing cations with approximately identical sizes: $NaZr_2(PO_4)_3$, $Ca_{0.5}Zr_2(PO_4)_3$, and $Nd_{1/3}Zr_2(PO_4)_3$. The rules governing the variations of the Nasicon type phosphate parameters have been reported previously (15). The value of the c parameter results from the influence of the Coulombic attraction between the cation in M_1 and the surrounding oxygens and the O^{2-}–O^{2-} repulsion occurring when M_1 is empty. Clearly the second factor prevails.

Assuming the fractional atomic coordinates are those of $NaZr_2(PO_4)_3$ (10), the mean rare earth–oxygen distances can be estimated. The calculated distances range from 2.55 Å (La) to 2.51 Å (Yb). These values are significantly larger than those predicted using the tables of ionic radii (16) which range between 2.43 Å (La) and 2.26 Å (Yb).

TABLE 2
Experimental and Calculated Densities of $Ln_{1/3}Zr_2(PO_4)_3$ (Ln = La, Nd, Eu, Gd)

$Ln_{1/3}Zr_2(PO_4)_3$	d_{exp} ± 0.03	d_{th}
Ln = La	3.25	3.33
Ln = Nd	3.28	3.35
Ln = Eu	3.34	3.38
Ln = Gd	3.33	3.40

TABLE 3
Comparison of the Structural Data of $NaZr_2(PO_4)_3$, $Ca_{0.50}Zr_2(PO_4)_3$, and $Nd_{1/3}Zr_2(PO_4)_3$

	(a_H ± 0.005) Å	(c_H ± 0.03) Å
$NaZr_2(PO_4)_3$ (10)	8.804	22.76
$Ca_{0.5}Zr_2(PO_4)_3$ (12)	8.805	22.85
$Nd_{1/3}Zr_2(PO_4)_3$	8.762	23.04

Actually the iono covalent character of these *RE*–O bonds can be discussed by taking into account some aspects of the luminescence spectra.

The $^5D_0 \rightarrow {}^7F_0$ transition energy of the Eu^{3+} emission recorded at 80 K in the europium zirconium phosphate is located at 17,355 cm^{-1}. The $^6P_{7/2} \rightarrow {}^8S_{7/2}$ transitions of the Gd^{3+} emission in the gadolinium zirconium phosphate recorded at 80 K are located at 32,208, 32,108, and 31,963 cm^{-1}, and the energy of the barycenter is 32,093 cm^{-1}.

All these values can be compared with the characteristics of the gallates of olivine type, $\alpha CaLnGaO_4$, in which Eu^{3+} or Gd^{3+} are located in slightly distorted octahedral sites with approximately similar *RE*–O distances of about 2.50 Å (17, 18). In the lanthanum phase, Eu^{3+} occupies a site with a symmetry C_2 and the $^5D_0 \rightarrow {}^7F_0$ transition energy is 17,158 cm^{-1}. The barycenter of the $^6P_{7/2} \rightarrow {}^8S_{7/2}$ emission of Gd^{3+} located at a similar site in the $CaLa_{1-x}Gd_xGaO_4$ phase decreases as x increases and is located below 32,000 cm^{-1}.

The comparison between these two sets of data and their positions in the nephelauxetic scale (21, 22) implies a higher ionic character for the rare earth–oxygen bond in the case of the phosphates. This is the consequence of the strong covalency of the antagonistic P–O bond. In addition the location of the rare earth at the center of M_1 is questionable due to the existence of the electric dipolar forbidden $^5D_0 \rightarrow {}^7F_0$ and $^5D_0 \rightarrow {}^7F_2$ transitions in the europium emission spectrum.

For the discussion of this point, the luminescence spectra recorded at 80 K can be analyzed in terms of the symmetry of the rare earth site. The $^6P_{7/2} \rightarrow {}^8S_{7/2}$ spectrum of Gd^{3+} contains three lines. In the case of Eu^{3+}, neglecting some weak shoulders, the origin of which will be discussed later, the spectrum recorded at 80 K can be assumed in a first approximation to consist of a unique $^5D_0 \rightarrow {}^7F_0$ line (17,355 cm^{-1}), two $^5D_0 \rightarrow {}^7F_1$ lines (17,076 and 16,683 cm^{-1}), and three $^5D_0 \rightarrow {}^7F_2$ lines (16,458, 16,410, and 16,263 cm^{-1}) (Fig. 7).

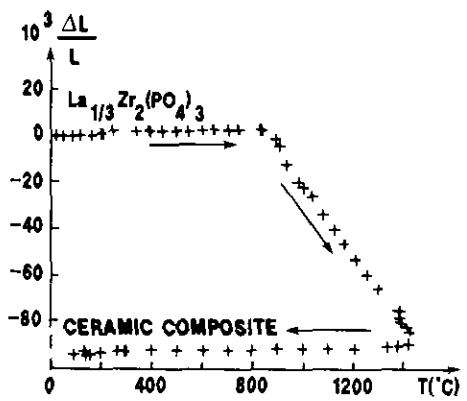

FIG. 9. Dilatometric curve of $La_{1/3}Zr_2(PO_4)_3$.

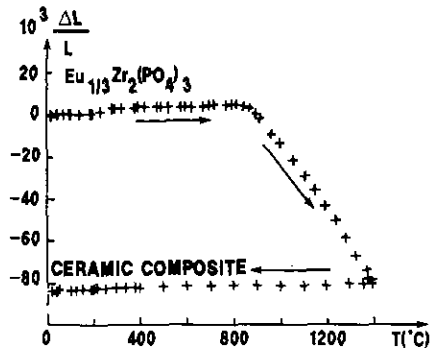

FIG. 10. Dilatometric curve of $Eu_{1/3}Zr_2(PO_4)_3$.

More specifically, the electric dipolar $^5D_0 \rightarrow {}^7F_2$ emission, which is hypersensitive to any deviation from centrosymmetry (19), can be readily detected. Thus the anionic environment is not strictly centrosymmetrical. Nevertheless, its intensity is weak, which excludes the location of Eu^{3+} in the strongly distorted M_2 site.

Finally, the crystal-field symmetry at the *RE* site can be assumed to be close to D_{3d}, which is the point group of the M_1 site in the $NaZr_2(PO_4)_3$ prototype.

The small intensity bands appearing at 16,580 cm^{-1} ($^5D_0 \rightarrow {}^7F_1$) and at 16,230 and 15,935 ($^5D_0 \rightarrow {}^7F_2$) likely indicate a distortion of the europium site itself or a slight displacement of the luminescent ion in an off-center position. They could be attributed as well to vibronic transitions of the overlapping $^5D_1 \rightarrow {}^7F_{3,4}$ manifolds.

III. DILATOMETRIC INVESTIGATION OF LANTHANUM AND EUROPIUM PHOSPHATES

A preliminary investigation of the thermal expansion properties has been undertaken for *Ln* = La and Eu. Dilatometric measurements were performed between room temperature and 1340°C using a Netzch 402 ED differential dilatometer. The samples were prepared as previously described and the powders were compacted to the initial stage in order to also follow the process of sintering.

Typical curves of dilatometric scans are given in Fig. 9 for $La_{1/3}Zr_2(PO_4)_3$ and in Fig. 10 for $Eu_{1/3}Zr_2(PO_4)_3$. Between room temperature and 870°C both materials exhibit a small, positive value of the mean thermal expansion coefficient: $\langle\alpha\rangle_{(La)} = 1.4 \times 10^{-6}\ °C^{-1}$ and $\langle\alpha\rangle_{(Eu)} = 2.0 \times 10^{-6}\ °C^{-1}$. Above 870°C, a strong shrinkage of the samples is observed which corresponds to the decomposition of the phosphates.

The so-called composites containing both the zirconium phosphate $Zr_2P_2O_9$ and the lanthanum or europium monophosphate exhibit a remarkable near-zero thermal expansion, shown by cooling the samples between 1340°C and

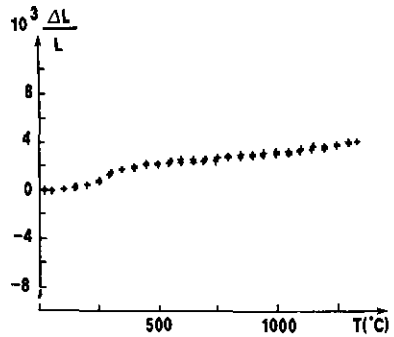

FIG. 11. Dilatometric curve of the ceramic composite (Ln = Eu).

room temperature, $\langle\alpha\rangle = 3 \times 10^{-7}$ °C^{-1} for the lanthanum ceramic composite and 1×10^{-7} °C^{-1} for the europium ceramic composite. Successive heating and cooling cycles can be carried out without observable hysteresis (Fig. 11). These preliminary results need additional "ceramic" investigations, which are presently in progress, to decide whether or not such composites could have a technological significance.

CONCLUSION

The new family of Nasicon type phosphates $Ln_{1/3}Zr_2(PO_4)_3$ (Ln = Rare Earth) has been prepared through a sol–gel route. The crystallization process was investigated by using Eu^{3+} and Gd^{3+} as structural local probes. Moreover, this technique allows identification of the strong ionic character of the rare earth–oxygen bond.

These phosphates decompose just below 900°C. This process is completely achieved at about 1400°C. In the case of La and Eu, the resulting material composites show a remarkably low thermal expansion over a rather large temperature range (RT → 1340°C).

REFERENCES

1. J. Alamo and R. Roy, *J. Am. Ceram. Soc.* **5,** C78 (1984).
2. R. Roy, D. K. Agrawal, J. Alamo, and R. A. Roy, *Mater. Res. Bull.* **19,** 471 (1984).
3. G. E. Le Nain, H. A. McKinstry, S. Y. Li Maye, and A. Woodward, *Mater. Res. Bull.* **19,** 1451 (1984).
4. R. Roy, E. R. Vance, and J. Alamo, *Mater. Res. Bull.* **17,** 585 (1982).
5. J. Alamo and R. Roy, *J. Mater. Sci.* **21,** 444 (1986).
6. T. Oota and I. Yamai, *J. Am. Ceram. Soc.* **69**(1), 1 (1986).
7. R. M. Hazen and C. T. Prewitt, *Amer. Mineral.* **62,** 309 (1977).
8. A. El Jazouli and J. M. Heintz, private communication.
9. B. E. Taylor, A. D. English, and T. Berzins, *Mater. Res. Bull.* **21,** 171 (1977).
10. L. O. Hagman and P. Kierkegaard, *Acta Chem. Scand.* **22,** 1822 (1968).
11. M. Sljukic, B. Matkovic, B. Prodic, and D. Anderson, *Z. Kristallogr.* **130,** 148 (1969).
12. D. K. Agrawal and V. S. Stubichn, *Mater. Res. Bull.* **20,** 99 (1985).
13. S. Y. Li Maye, D. K. Agrawal, and H. A. McKinstry, *J. Am. Ceram. Soc.* **70**(10), C232 (1987).
14. M. Alami, R. Brochu, C. Parent, L. Rabardel, and G. Le Flem, *J. Alloys Comp.* **118,** 117 (1992).
15. F. Cherkaoui, J. C. Viala, C. Delmas, and P. Hagenmuller, *Solid State Ionics* **21,** 333 (1986).
16. R. D. Shannon, *Acta Crystallogr. Sect. A* **32,** 75 (1976).
17. H. Ronde, D. M. Krol, and G. Blasse, *J. Electrochem. Soc.* **124**(8), 1276 (1977).
18. J. Fava, Nguyen-Trut-Dinh, and G. Le Flem, *Mater. Res. Bull.* **14,** 683 (1979).
19. C. Linares, M. Blanchard, and F. Gaume-Mahn, *in* "Proceedings, 7th Rare Earth Symposium." Nauka, Moscow, 1972.
20. M. Zahir, R. Olazcuaga, C. Parent, G. Le Flem, and P. Hagenmuller, *J. Non-Cryst. Solids* **69,** 221 (1985).
21. P. Caro, O. Beaury, and E. Antic, *J. Phys.* **37,** 671 (1976).
22. P. Caro, E. Antic, L. Beaury, O. Beaury, J. Derouet, M. Faucher, C. Gutter, O. K. Moune, and P. Porcher, *Colloq. C.N.R.S. de Lyon* **255,** 71 (1976).
23. S. Senbhagaraman and A. M. Umarji, *J. Solid State Chem.* **85,** 169 (1990).